RESEARCH ARTICLE

Check for updates

Exploring protonation sites with cation-responsive polyethylene glycol (PEG) tethers in [FeFe]-hydrogenase mimics†‡

Alejandro Torres, [iD] [a,b] Sergio Aguado, [iD] [a,b] Alba Collado, [iD] [b,c,d] Elena Sáez, [iD] [e] Mar Gómez-Gallego [iD] [a,b] and Miguel A. Sierra [iD] *[a,b]

Mimics of [FeFe]-hydrogenases having two [(μ-adt)Fe$_2$(CO)$_6$] moieties linked through 1,2,3-triazole rings with polyethylene glycol (PEG) chains [(−OCH$_2$CH$_2$O−)$_4$ (**7**) and (−OCH$_2$CH$_2$O−)$_5$ (**8**)] are able to coordinate to alkali ions (Na$^+$, K$^+$) *via* the *O*-PEG atoms and the triazole-*N*3 positions. Electrocatalytic studies in trifluoroacetic acid (TFA) demonstrate that their catalytic performance is affected by the presence of Na$^+$ and K$^+$ salts. The addition of NaPF$_6$ decreases the electrocatalytic activity of **7** and **8** (about 50% reduction of the TOF values). As, in TFA, **7** and **8** could be protonated in both the triazole and adt-amino groups, the reduction in TOF values suggests that NaPF$_6$ inhibits the contribution of the triazolium species to the electrocatalytic process, likely due to the involvement of the triazole-*N*3 positions in Na$^+$ binding. However, the addition of KPF$_6$ either does not change (**7**) or increases the TOF values (**8**). ^{1}H NMR titration experiments demonstrate that, despite the presence of K$^+$ ions in the media, triazolium salts are formed. Therefore, the TOF values should reflect the contribution of species protonated in both the triazole and adt-amino groups to the HER process.

Introduction

[FeFe]-hydrogenases ([FeFe]-H$_2$ases) are metalloenzymes featuring a bimetallic complex composed of two iron atoms linked by an azadithiolate (adt) bridged ligand, to which a [Fe$_4$S$_4$] cluster is attached through cysteine sulfur atoms (**1** in Fig. 1).[1] The metal core completes the coordination sphere with CO and CN$^-$ ligands.[2] While the [Fe$_4$S$_4$] cluster plays a fundamental role in electron transport, the adt bridge is responsible for providing/removing protons due to the basic properties of the secondary amine.[3] Diiron hexacarbonyl com-

plexes of general formula [(μ SR)$_2$Fe$_2$(CO)$_6$] (**2**) are considered [FeFe]-H$_2$ase mimics, as they exhibit significant structural similarities with the active center of enzymes **1**[4] and also show an analogous acid–base and redox behavior.[5] In mimics **2**, the iron centers of the [FeFe] subsite have a formal oxidation state of +1, form a single Fe–Fe bond (~2.5 Å)[6] and complete their coordination sphere with CO ligands. Depending on the substituents on the dithiolate bridgehead, these complexes belong to two different structural classes: complexes of general structure **3** have an adt bridge (as in natural enzymes **1**), while complexes such as **4** (propanedithiolate bridge, pdt) and **5** (benzenedithiolate bridge, bdt) have all-carbon chains between the sulfur atoms[5] (Fig. 1).

The hydrogen evolution reaction (HER) in **1** and [FeFe]-hydrogenase mimics is a two-proton/two-electron reduction process, but the mechanistic steps differ depending on the type of mimic (**3**, **4**, **5**) and the catalytic conditions.[7] The introduction of additional basic centers in pdt- and bdt-[FeFe]-H$_2$ase mimics has been recognized as beneficial for the electrocatalytic properties of these molecules, and this effect has been studied.[8] It is known that the HER cycle is facilitated by the initial protonation of an additional basic site[8h] and is also favored by the presence of basic substituents (*i.e.* phosphines) that increase the basicity of the metal centers.[8d,i] In natural [FeFe] and [NiFe]-hydrogenase enzymes, the protonation of one of the cysteinyl thiolate substituents of the [Fe$_4$S$_4$]

[a]Departamento de Química Orgánica, Facultad de Química, Universidad Complutense, 28040-Madrid, Spain. E-mail: sierraor@ucm.es
[b]Centro de Innovación en Química Avanzada (ORFEO-CINQA), Departamento de Química Orgánica, Facultad de Química, Universidad Complutense, 28040-Madrid, Spain
[c]Departamento de Química Inorgánica, Universidad Autónoma de Madrid, 28049 Madrid, Spain
[d]Institute for Advanced Research in Chemical Sciences (IAdChem), Universidad Autónoma de Madrid, 28049 Madrid, Spain
[e]Unidad de Resonancia Magnética, Facultad Ciencias Químicas, Universidad Complutense, 28040-Madrid, Spain

4480 | *Inorg. Chem. Front.*, 2025, **12**, 4480–4493
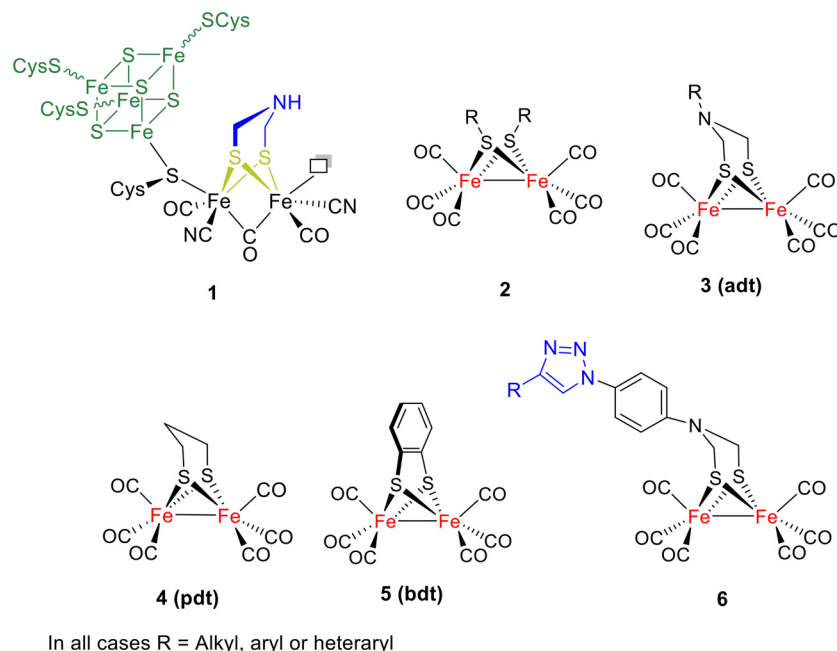
This journal is © the Partner Organisations 2025

Fig. 1 The schematic representation of a [FeFe]-H$_2$ase active center and the main synthetic mimics.

cluster has been proposed as a key step in the catalytic cycle.[8a,k,l] Also, in [FeFe]-hydrogenases, it has been demonstrated that the strongly conserved secondary ligand sphere around the (2Fe$_H$) cluster plays a major role in preserving a stable cofactor coordination and geometry, favoring the stabilization of the CN-ligands.[8m] However, while the protonation of the N atom of the adt bridge is generally accepted to be the first step in the HER cycle for adt-[FeFe] mimics, the influence of additional basic centers in the process has been less explored. In this regard, recent work by our group showed that the basic 1,2,3-triazole ring in complex **6** (Fig. 1) can be protonated with a strong acid (H$_2$SO$_4$), and the formation of the triazolium species considerably enhances the electrocatalytic activity of the complex.[9]

The incorporation of secondary metal ions has emerged as an attractive strategy to tune chemical properties and to observe new reactivity patterns in metal complexes.[10,11] In fact, recent attention has been paid to the study of the effect of adding redox-inactive metal ions (*i.e.* Li$^+$, Na$^+$, K$^+$, Ca^{2+}), as a way to modulate the electrochemical properties of a metal complex.[10b,e] Inspired by this idea, we devised compounds **7** and **8**, which combine two [(μ-adt)Fe$_2$(CO)$_6$] moieties linked by polyethylene glycol (PEG) chains of different lengths, through 1,2,3-triazole rings (Fig. 2). The coordination of **7** and **8** to alkali ions (Na$^+$, K$^+$) must involve the O-PEG and the basic triazole-$N3$ atoms.[12] In these complexes, we should be able to control the participation/inhibition of the triazole rings in cation binding by acid addition, modulating the electrochemical properties. Therefore, the study of the electrochemical response of **7** and **8** in the presence/absence of Na$^+$ or K$^+$ salts in acid media will allow us to determine the contri-
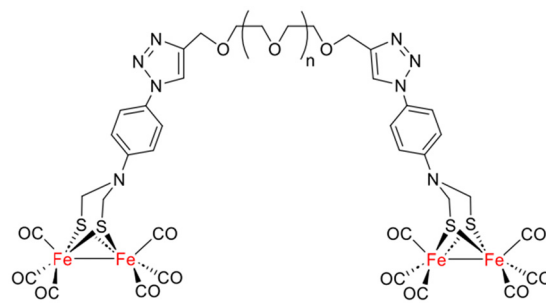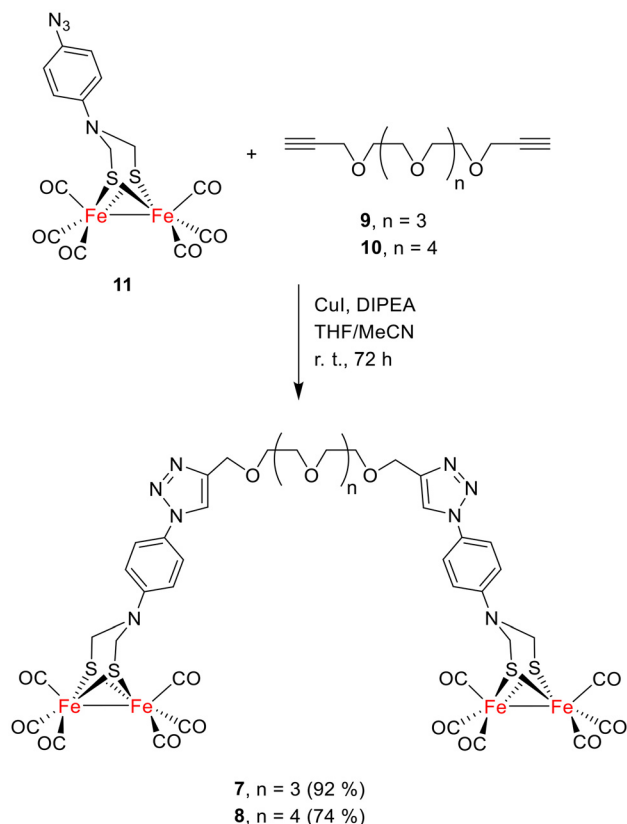

Fig. 2 The structure of the compounds **7** (n = 3) and **8** (n = 4) studied in this work.

bution of the N-amino-adt *versus* $N3$ triazole-protonated species to the HER process.

Results and discussion

The synthesis of [FeFe]-H$_2$ase mimetics **7** and **8** was achieved by a cycloaddition reaction between alkynes **9** and **10** and azide **11**, catalyzed by Cu(I) (Scheme 1).[13] The synthesis of azide **11** was previously described by us.[9] Meanwhile, alkynes **9**[14] and **10**[15] were prepared by reacting the corresponding commercially available diols with propargyl bromide and NaH in THF at room temperature. Compounds **7** and **8** were obtained in 92% and 74% yields, respectively, after column chromatography (SiO$_2$, CH$_2$Cl$_2$/MeOH 95 : 5) and were characterized by spectroscopic techniques. Significant in the NMR

This journal is © the Partner Organisations 2025

Inorg. Chem. Front., 2025, **12**, 4480–4493 | **4481**

Scheme 1 Preparation of the tetrametallic complexes **7** and **8**.

Fig. 3 ^{1}H NMR spectra (500 MHz) of complexes **7** (left) and **8** (right) upon the addition of 4 equiv. of NaPF$_6$ (in green) and KPF$_6$ (in red) in CD$_3$CN at 25 °C. The signal at 3.55 ppm (*) was used as reference in the study.

spectra of **7** and **8** are the signals attributable to the CH of the newly formed 1,2,3-triazole rings at 7.96 ppm in the ^{1}H NMR and 120.9 ppm in the ^{13}C{^{1}H} NMR spectra.

Coordination studies with alkali metal cations

The ability of complexes **7** and **8** to coordinate to alkali metal cations was evaluated by ^{1}H-NMR. The polyethylene glycol (PEG) bridges in compounds **7** and **8** are analogous to those of 15-crown-5 and 18-crown-6 ethers, which have cavity diameters of 1.7–2.2 Å and 2.6–3.2 Å, respectively, capable of forming 1 : 1 coordination complexes with Na$^+$ and K$^+$.[16] Coordination studies were performed in solutions of complexes **7** and **8** in CD$_3$CN with increasing concentrations of NaPF$_6$ or KPF$_6$ (0–4 equivalents). The selection of NaPF$_6$ and KPF$_6$ as cation sources was based on their higher solubility under the experimental conditions. In all cases, in the ^{1}H NMR spectra, the signals of the PEG fragments were shifted to lower fields as the cation concentration increased, indicating cation coordination to the oxygen atoms (Fig. 3). The most affected signals were those of the four central methylene protons of the polyether units (singlets at 3.55 ppm and 3.54 ppm, for **7** and **8**, respectively, in Fig. 3), which served as references for the subsequent calculations. Fig. 4 shows the plots of $\Delta\delta$ (ppm) *versus* the amounts of Na$^+$ and K$^+$ for compounds **7** and **8**. The plots reveal a steady increase in $\Delta\delta$ values until the stationary region is reached, indicating saturation. Job plots were constructed
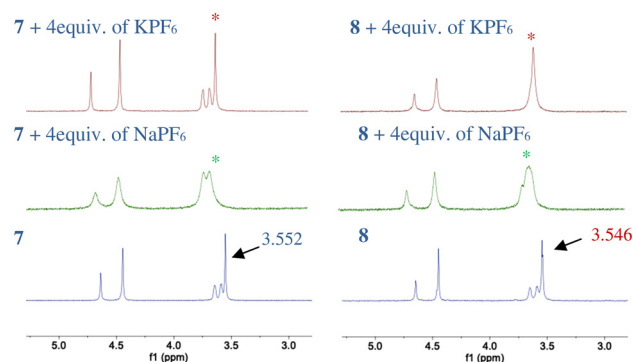
from the ^{1}H NMR data to determine the stoichiometry of the complexes (Fig. 5), with maxima at χ^1 and χ^2 = 0.5, suggesting a 1 : 1 stoichiometry for the metal cation coordination complexes.[17]

Once the stoichiometry of coordination complexes was known, the association constants (K_a, M^{-1}) of the different equilibria were calculated following the reported procedure.[17] Experimental K_a values in CH$_3$CN for [**7**-Na$^+$] and [**7**-K$^+$] were 6.66 × 10^2 M^{-1} and 1.16 × 10^3 M^{-1}, respectively, while for [**8**-Na$^+$] and [**8**-K$^+$], they were 8.49 × 10^2 M^{-1} and 1.63 × 10^3 M^{-1}, respectively. The calculated association constants are about two orders of magnitude higher than those obtained for analogous acyclic polyethers in the presence of Na$^+$ and K$^+$, which highlights the ability of **7** and **8** to bind sodium and potassium and points to the participation of the triazole $N3$ positions in the process.[17,18]

Additional support for the structures of the alkali complexes was obtained using DFT calculations at the SMD (CH$_3$CN)-M06/6-31G** level. As shown in Fig. 6, in [**7**-Na$^+$], the cation is coordinated to seven donor atoms: the five O (PEG) atoms and the two triazole $N3$ atoms. The Na–O distances fit well with the expected Na–O distance (2.42 Å), and the Na–N distances (2.48 Å and 2.65 Å, respectively) agree with the expected Na–N distance (2.54 Å), which confirms the strong interaction between the sodium ion and the $N3$ positions of both triazole rings. In turn, in the potassium complex [**7**-K$^+$], the cation is coordinated to the five O positions of the PEG moiety (K–O average distance of 2.72 Å) and to one of the triazole $N3$ atoms (K–N distance of 2.83 Å), in a pseudo-crown-6 structure, with K–O and K–N distances in the range of the expected values (K–O 2.78 Å and K–N 2.80 Å, respectively). The remaining triazole ring is positioned above the macrocycle at a distance of K–$N3$ of 3.08 Å.

The computed structures of [**8**-Na$^+$] and [**8**-K$^+$] are depicted in Fig. 7. In both cases, the $N3$ positions of the triazole fragments are deeply involved in the coordination to the alkali cations together with the PEG fragments. For complex [**8**-Na$^+$], the average distance Na–O is 2.68 Å and the Na–$N3$ distances
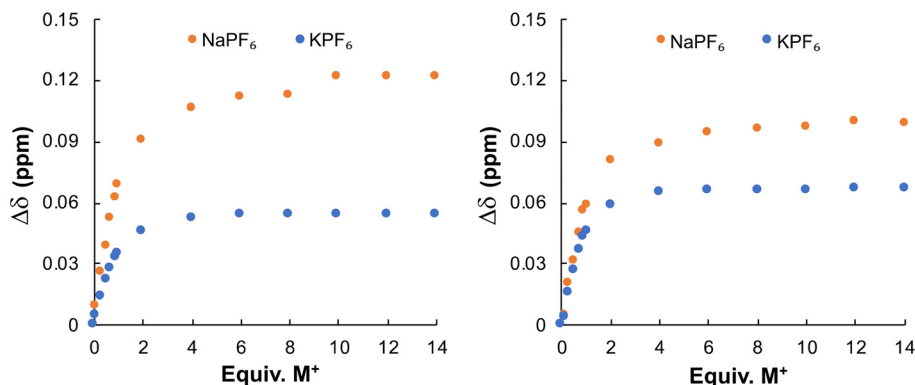
4482 | *Inorg. Chem. Front.*, 2025, **12**, 4480–4493

This journal is © the Partner Organisations 2025

Fig. 4 Representation of $\Delta\delta$ (ppm) *vs.* equivalents of Na$^+$ and K$^+$ for **7** (left) and **8** (right) at 25 °C.
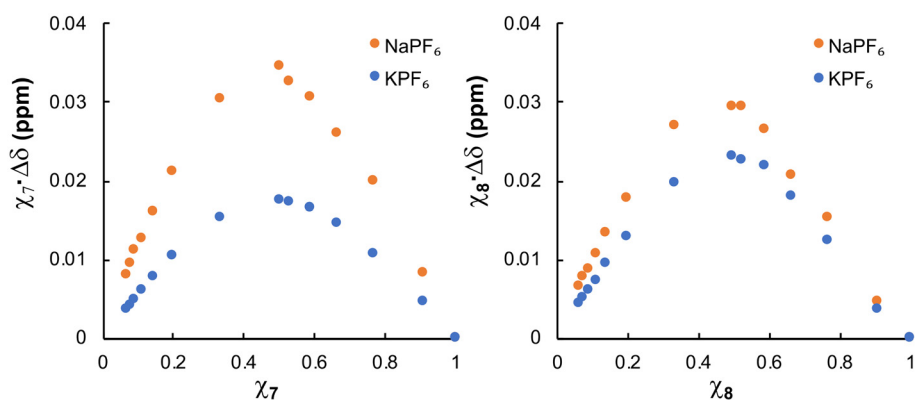

Fig. 5 Job plots of compounds **7** (left) and **8** (right) with NaPF$_6$ and KPF$_6$ at 25 °C.

Fig. 6 Calculated structures of complexes [**7**-Na$^+$] (top) and [**7**-K$^+$] (bottom) (SMD (CH$_3$CN)-M06/6-31G** level). Hydrogen atoms have been omitted for clarity. Bond distances in Å. Na−N and K−N distances are shown in red.
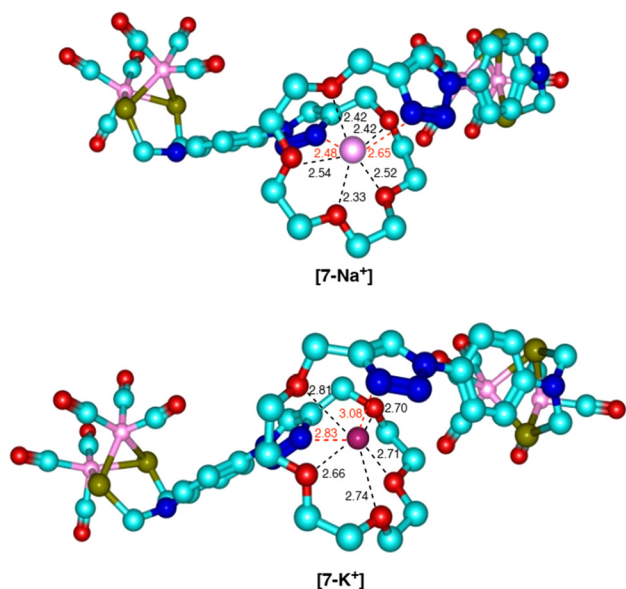
Fig. 7 Calculated structures of complexes [**8**-Na$^+$] (top) and [**8**-K$^+$] (bottom) (SMD (CH$_3$CN)-M06/6-31G** level). Hydrogen atoms have been omitted for clarity. Bond distances in Å. Na−N and K−N distances are shown in red.
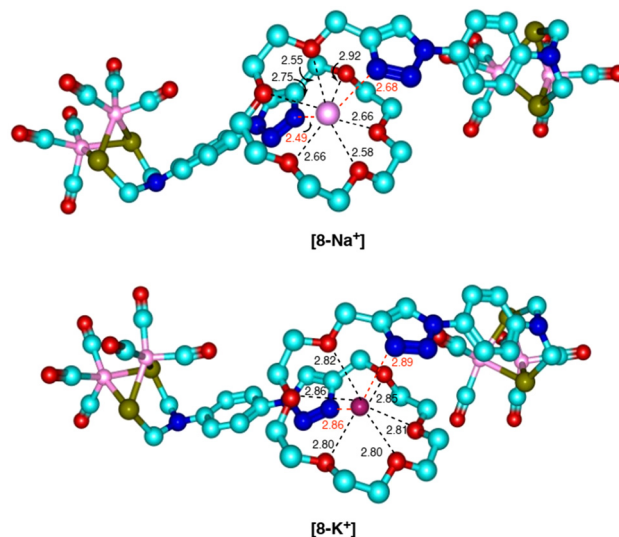
are 2.49 Å and 2.68 Å, respectively. In turn, for complex [**8**-K$^+$], the average K–O distance is 2.82 Å and the Na–N3 distances are 2.89 Å and 2.85 Å, all within the range of the literature data.[19]

Electrochemistry

The electrochemical and electrocatalytic properties of compounds **7** and **8** and their Na$^+$ and K$^+$ coordination complexes were explored. Compounds **7** and **8** exhibited similar electrochemical behavior. Both showed a reduction wave at E_{pc} = −1.57 V attributed to the [Fe^{I}Fe^I]/[Fe^{0}Fe^I] process in the [(μ-adt)Fe$_2$(CO)$_6$] moieties, together with an irreversible second reduction wave at E_{pc} = −2.18 V, corresponding to the [Fe^{0}Fe^I]/[Fe^{0}Fe^0] process in the same fragment (Fig. 8).[20]

In the presence of a weak acid (AcOH), **7** and **8** display the expected behavior for a [(μ-adt)Fe$_2$(CO)$_6$] derivative.[21] The band at −1.56 V does not change, but the intensity of the second reduction wave at −2.18 V steadily increases with the successive additions of acid (Fig. 9, top). Upon the addition of the stronger trifluoroacetic acid (TFA, pK_a^{MeCN} ≈ 12.6), there is a clear electrocatalytic response of the wave at −1.56 V (Fig. 9, bottom). However, at high concentrations of acid (6–10 equiv.), the catalytic current (i_{cat}) at −2.18 V also increases. In agreement with our previous results, the electrocatalytic behavior observed for **7** and **8** in TFA must be due to the contribution of the species protonated in both the triazole ring and the adt-amino groups.[8] The i_{cat}/i_p plots vs. increasing acid concentrations were used to evaluate the electrocatalytic properties of **7** and **8** in the reduction of protons from TFA (i_p is the peak current in the absence of acid, Fig. 10). The data revealed that
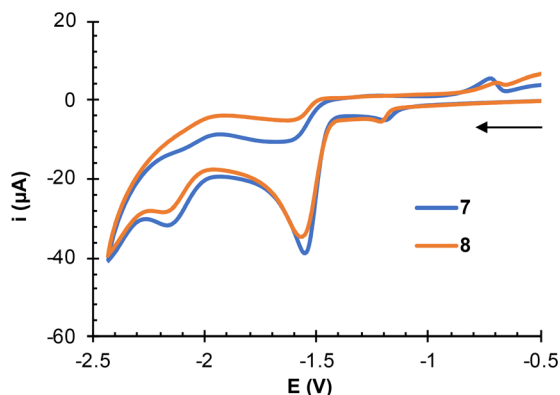

Fig. 8 Cyclic voltammograms of complexes **7** and **8** in a 10^{-3} M MeCN solution containing [(^{n}Bu)$_4$N]PF$_6$ 10^{-1} M as the supporting electrolyte. Voltammograms were registered at 25 °C using a Pt counter electrode and a glassy carbon working electrode. Potentials are given in V vs. Fc$^+$/Fc. Scan rate: 100 mVs.
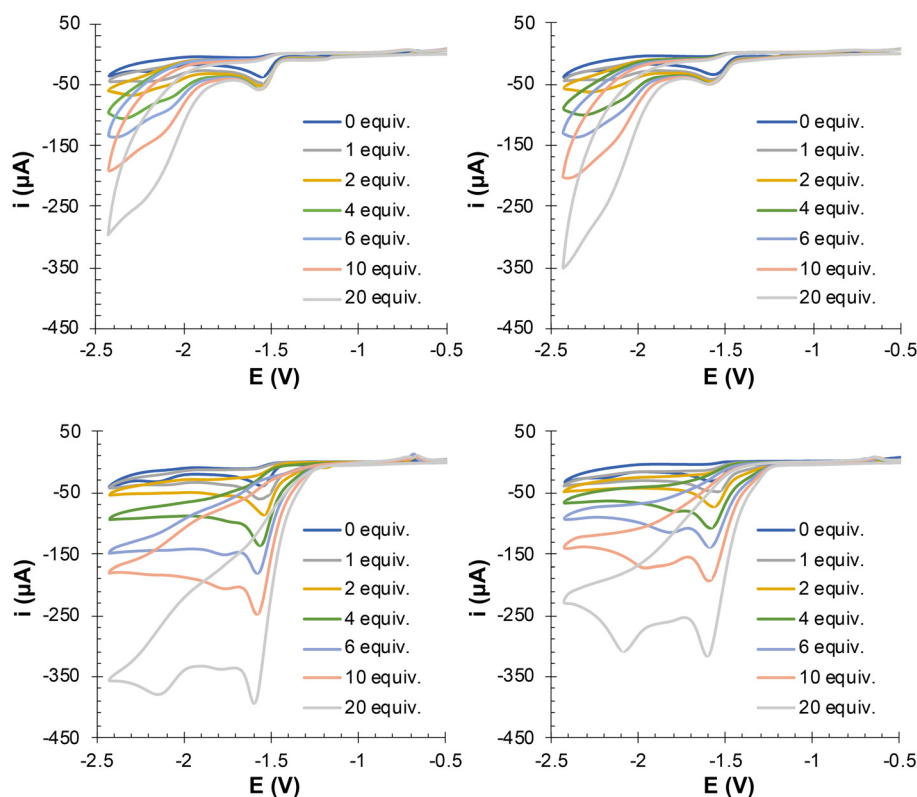
Fig. 9 CVs of compounds **7** (left) and **8** (right) with increasing amounts of AcOH (top) and TFA (bottom) obtained from 10^{-3} M solutions in MeCN containing [(^{n}Bu)$_4$N]PF$_6$ 10^{-1} M as the supporting electrolyte, recorded at 25 °C. Counter-electrode: Pt; working electrode: glassy carbon; potentials given in V vs. Fc$^+$/Fc; scan rate: 100 mV s^{-1}.

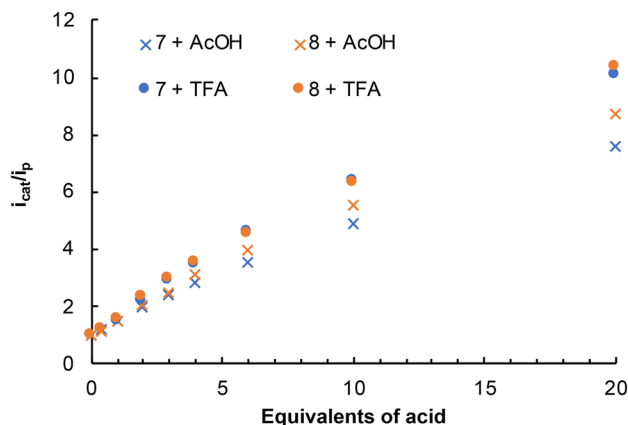**4484** | *Inorg. Chem. Front.*, 2025, **12**, 4480–4493

This journal is © the Partner Organisations 2025

Fig. 10 Representation of i_{cat}/i_p of **7** and **8** vs. equivalents of AcOH and TFA.

8 displayed a higher (about 15% more) electrocatalytic activity than **7** with AcOH, but their performance was similar with TFA.

To determine the effect of cation binding on the process, the cyclic voltammograms (CVs) of **7** and **8** were recorded in the presence of $NaPF_6$ or KPF_6 (5 equiv.) (Fig. 11). Compared to the CVs of **7** and **8**, the current intensity of the first reduction wave increased for both [**7-Na$^+$**] and [**8-Na$^+$**] but slightly decreased for the potassium complexes. However, the second reduction wave that appeared at −2.18 V in the CV of the uncoordinated compounds was significantly altered by the nature of the cation. The CV of complex [**7-Na$^+$**] displayed a crossover upon reversing the potential scan direction, likely due to the deposition of insoluble material on the working electrode. In contrast, complex [**8-Na$^+$**] showed no such deposition. This displacement has been observed previously in different transition metal complexes bearing crown ether moieties.[22]

The electrocatalytic activity of **7** and **8** in the presence of 5 equiv. of $NaPF_6$ or KPF_6 and with increasing amounts of TFA (1–20 equiv.) was next addressed (Fig. 12). The i_{cat}/i_p plots and

the turnover frequency (TOF s^{-1}) values for the [Fe^{I}Fe^I]/[Fe^{I}Fe^0] reduction wave, with 20 equiv. of TFA, were used to evaluate the electrocatalytic activity of the complexes (Fig. 13 and Table 1). The calculated overpotential was 0.68 V. The results revealed that, in TFA, the electrocatalytic activity of **7** and **8** in the presence of $NaPF_6$ was considerably diminished, as indicated by the 50% reduction in the TOF values. As compounds **7** and **8** could be protonated in both the triazole rings and the adt-amino groups,[9] the reduction in the TOF values suggests that the contribution of the triazolium species to the electrocatalytic process is inhibited with $NaPF_6$. Undoubtedly, despite the addition of acid, complexes [**7-Na$^+$**] and [**8-Na$^+$**] are formed in the medium, with the N3 positions of the triazole rings involved in the Na$^+$ binding.

These assertions were confirmed by an ^{1}H NMR study carried out with complex **8**. The spectra in Fig. 14 show the protonation of the triazole rings in compound **8** as the amount of TFA increased in solution (0–10 eq.) The formation of the triazolium salt causes the broadening and the significant downfield shift of the H5 signal of the triazole due to a rapid proton exchange between the protonated centers in the triazole-PEG region.[9] The signals corresponding to the [(μ-adt) Fe$_2$(CO)$_6$] fragment (7.70, 6.96 and 4.45 ppm) are hardly affected by the addition of acid, which suggests that protonation is specific to the triazole moiety. When the titration with TFA was done in the presence of $NaPF_6$, the ^{1}H NMR spectra of **8** changed significantly (Fig. 15). Unlike the free complex, the signals corresponding to the triazole fragment remain sharp and barely shift as the TFA concentration increases. This indicates that the triazole-PEG region does not undergo rapid proton exchange when Na$^+$ is present, supporting the formation of the coordination complex [**8-Na$^+$**] in the acid media.

The electrochemical experiments of **7** and **8** with the potassium salt in the presence of TFA had a different outcome. Data for compound **7** in Fig. 12 and 13 and Table 1 indicate a similar electrocatalytic response in the presence or absence of KPF_6 (TOF values of 20.4 s^{-1} and 19.9 s^{-1}, respectively). However, the addition of the potassium salt in TFA enhances the electrocatalytic activity of **8** (TOF values of 21.0 s^{-1} versus
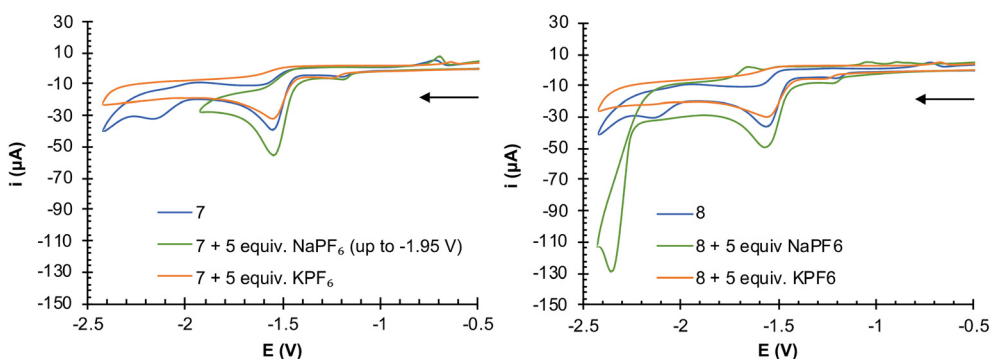
Fig. 11 CVs of compounds [**7-Na$^+$**], [**7-K$^+$**], [**8-Na$^+$**] and [**8-K$^+$**] obtained from 10^{-3} M solutions in MeCN containing [(^{n}Bu)$_4$N]PF$_6$ 10^{-1} M as the supporting electrolyte, recorded at 25 °C. Counter-electrode: Pt; working electrode: glassy carbon; potentials given in V vs. Fc$^+$/Fc; scan rate: 100 mV s^{-1}.

This journal is © the Partner Organisations 2025

Inorg. Chem. Front., 2025, **12**, 4480–4493 | **4485**

Fig. 12 CVs of (a) complex **7** with TFA + 5 equiv. of NaPF$_6$, (b) complex **8** with TFA + 5 equiv. of NaPF6, (c) complex **7** with TFA + 5 equiv. of KPF$_6$, and (d) complex **8** with TFA + 5 equiv. of KPF$_6$, obtained from 10^{-3} M solutions in MeCN containing [(^{n}Bu)$_4$N]PF$_6$ 10^{-1} M as the supporting electrolyte, recorded at 25 °C. Counter-electrode: Pt; working electrode: glassy carbon; potentials given in V vs. Fc$^+$/Fc; scan rate: 100 mV s^{-1}.

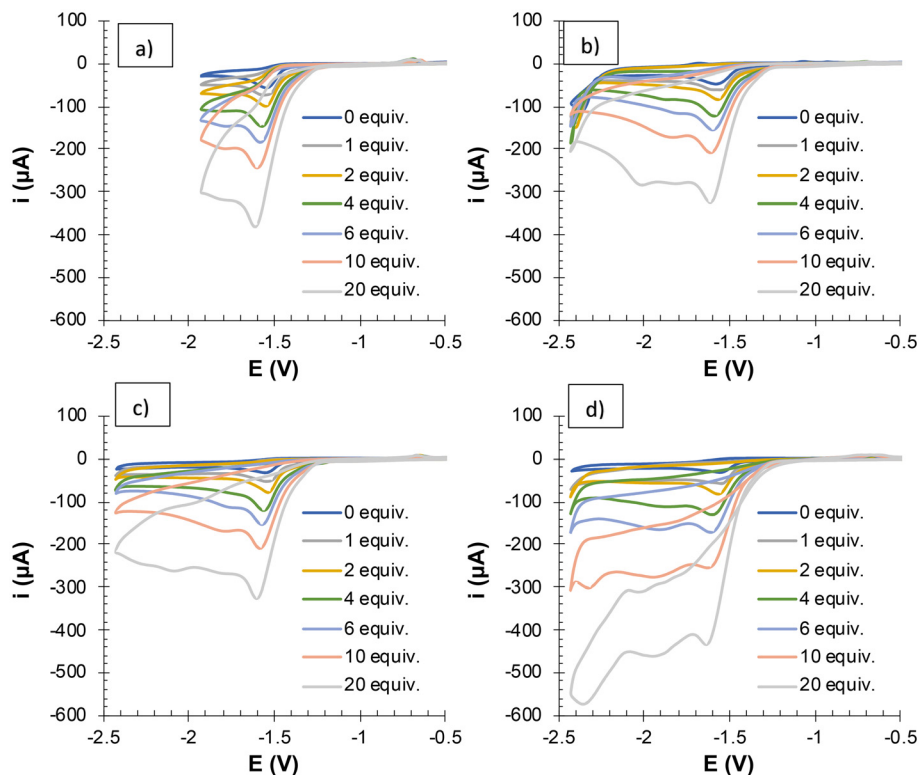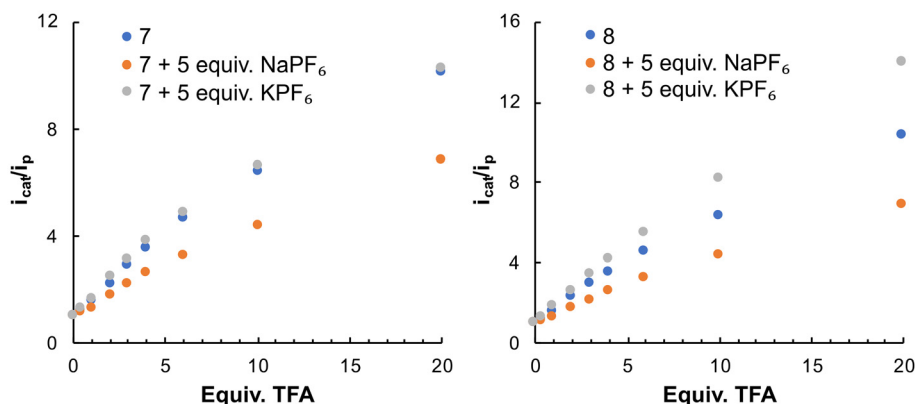**Fig. 13** Representation of i_{cat}/i_p of complexes **7** and **8** with 5 equivalents of NaPF$_6$ and KPF$_6$ vs. equivalents of TFA.

37.9 s^{-1} with KPF$_6$). These experimental data suggest that the addition of KPF$_6$ does not hamper the protonation of the tri-azole rings of **7** and **8**. Obviously, in the presence of KPF$_6$, the triazole *N*3-positions are not involved in the coordination of K$^+$ in acid media. The TOF values in these cases should reflect the contributions of the species protonated in both the triazole rings and the adt-amino groups to the HER process.

The ^{1}H NMR spectroscopy study of complex **8** with KPF$_6$ in the presence of increasing amounts of TFA (0–10 eq.) sup-

Table 1 TOF data^{a,b}

	7	**7**/NaPF$_6$	**7**/KPF$_6$	**8**	**8**/NaPF$_6$	**8**/KPF$_6$
TOF (s^{-1})^c	19.9	9.0	20.4	21.0	9.2	37.9

^{a} Data obtained from Fig. 12 and 13. ^{b} $i_{cat} = -1.57$ V; overpotential (η) = 0.68 V, calculated using E_0(TFA) = 0.89 V. ^{c} TOF calculated with 20 equiv. of TFA.

Fig. 14 ^{1}H NMR spectra (300 MHz) of compound **8** with TFA (0–10 equiv.) in CD$_3$CN at 25 °C. Arrows indicate signals corresponding to the triazole-PEG fragment.
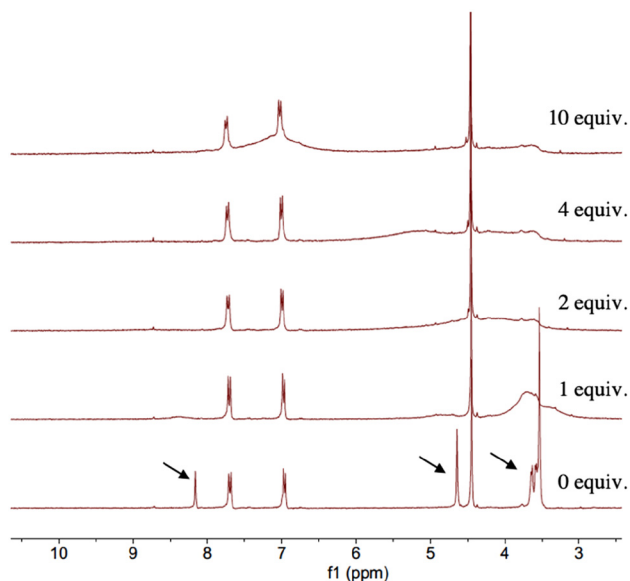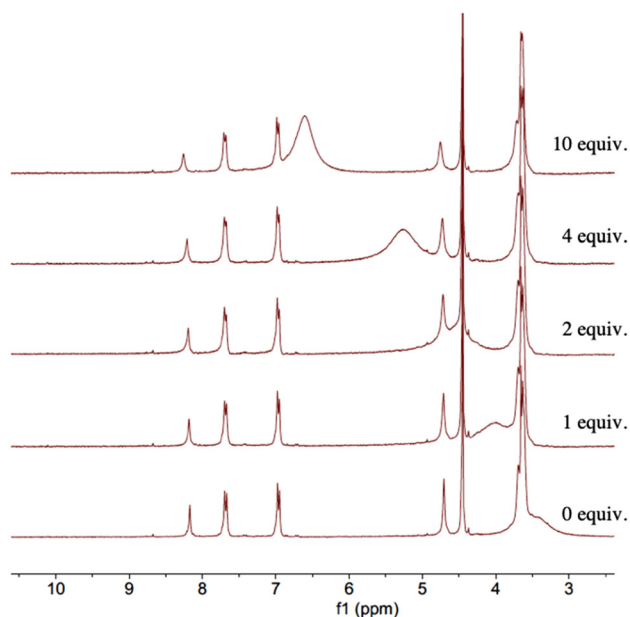

Fig. 15 ^{1}H NMR spectra (300 MHz) of compound **8** with 5 equiv. of NaPF$_6$ and TFA (0–10 equiv.) in CD$_3$CN at 25 °C.

ported these claims. As shown in Fig. 16, the signal of the *H*5 proton of the triazole ring broadens and experiences a significant downfield shift as the amount of TFA increases in solution. The process is almost identical to that observed in Fig. 14 for complex **8** in the presence of increasing amounts of TFA.

Additional insights into the coordinating behavior of complex **8** in trifluoroacetic acid media were obtained by determining its complexation constants using the same methodology
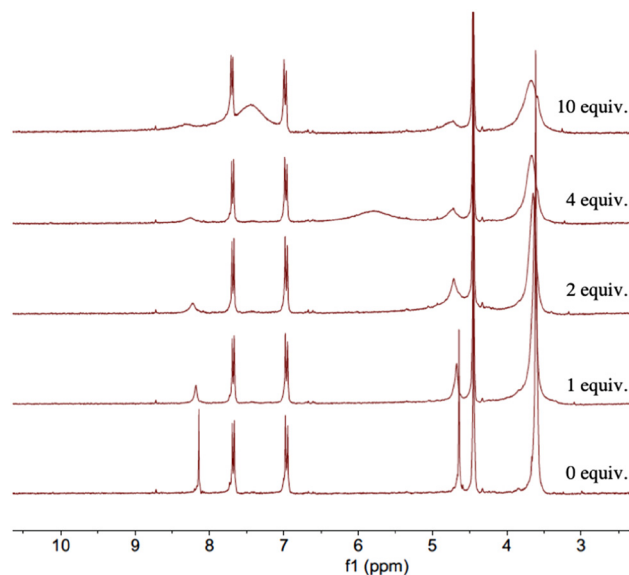

Fig. 16 ^{1}H NMR spectra (300 MHz) of compound **8** with 5 equiv. of KPF$_6$ and TFA (0–10 equiv.) in CD$_3$CN at 25 °C.

applied under neutral conditions, in the presence of 5 equivalents of TFA (see above and the ESI‡) and NaPF$_6$ and KPF$_6$. The data from Job's plots show that the ratio of ligand **8** to the alkali cation was 1 : 1 in both cases (Fig. S69‡). The association constants (K_a) in MeCN for **[8-Na$^+$ + TFA]** and **[8-K$^+$ + TFA]** were found to be 4.04×10^2 M^{-1} and 1.26×10^3 M^{-1}, respectively. As anticipated, these values were lower than those obtained under neutral conditions (6.66×10^2 M^{-1} and 1.63×10^3 M^{-1} for **[8-Na$^+$]** and **[8-K$^+$]**, respectively), since, under acidic conditions, the 1,2,3-triazole moiety is expected to be protonated, rendering it unavailable for coordination with the alkali metal cations.

The electrocatalytic and NMR experiments demonstrate the fundamental role of the alkali ions in modulating the electrocatalytic response of **7** and **8** in acid medium. With NaPF$_6$/TFA, the triazole units are engaged in the coordination with Na$^+$ and are not able to contribute to the HER process. The experimental TOF values of 9.0 s^{-1} for **7** and 9.2 s^{-1} for **8** in the presence of NaPF$_6$/TFA essentially show the contribution of the species protonated in the amino adt groups, whereas with KPF$_6$/TFA, the triazole units in **7** and **8** are protonated and can participate in the reaction.

It is well established that the protonated amine plays a fundamental role in the mechanism of hydrogen generation from $[(\mu\text{-adt})Fe_2(CO)_6]$ mimics, serving as a readily available source of protons for the neighboring Fe atom.[5b,7f,21a] Our results provide new insights into the contribution of *N*3-protonated 1,2,3-triazolium salts, which significantly enhance the electrocatalytic activity of $[(\mu\text{-adt})Fe_2(CO)_6]$ mimics in strong acidic media. While the protonated amine serves as a direct proton donor for the Fe atom, the *N*3-protonated 1,2,3-triazolium salts would provide an additional reservoir of protons, enhancing the overall catalytic efficiency. Although the potential role of
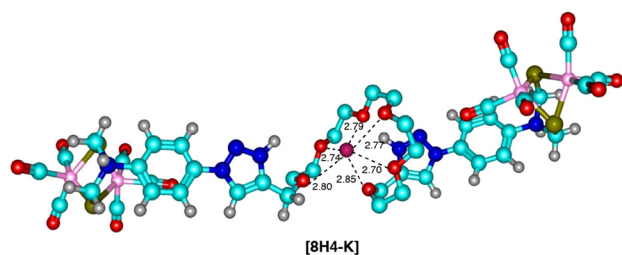
This journal is © the Partner Organisations 2025

Inorg. Chem. Front., 2025, **12**, 4480–4493 | **4487**

Fig. 17 Computed SMD (CH$_3$CN)-M06/6-31G** structure of [8H4-K]. The hydrogen atoms of the PEG linker have been omitted for clarity. Bond distances are in Å.

the 1,2,3-triazole moieties as electron reservoirs could also be considered, recent studies on [FeFe]H$_2$ase mimics with alkyl 1,2,3-triazolium salts as ligands exclude the triazolium ring as an additional redox-active site in the hydrogen evolution reaction (HER) process.[8e,f,9]

The observed increase in the turnover frequency (TOF) for compound **8** in trifluoroacetic acid (TFA) with KPF$_6$ (37.9 s^{-1}) compared to the TOF for compound **8** without the potassium salt (21.0 s^{-1}) remains unclear. Experimental evidence indicates that the triazole rings are protonated in both cases and can contribute to the HER process together with the protonated amino adt groups. A computational study would shed some light on this question. The SMD (CH$_3$CN)-M06/6-31G** computed structure of **8**, protonated in both the triazole and [(μ-adt)Fe$_2$(CO)$_6$] amino groups [8H4-K], reveals the six PEG oxygen atoms coordinated to K$^+$ in a very regular pseudo-18-crown-6 structure (Fig. 17). The average K–O distance in the hexacoordinated potassium complex is 2.77 Å, in excellent agreement with the expected K–O distance (2.78 Å), calculated as the sum of the oxygen van der Waals radius (1.40 Å) and the effective ionic radius of K$^+$ (1.38 Å).[23] The incorporation of alkali metal ions is known to enhance the electrocatalytic activity of metal complexes,[10,11] and the formation of the coordination complex [8H4-K] could account for the increased TOF observed for compound **8** in TFA in the presence of KPF$_6$. The fact that the TOF values for complex **7** in TFA are almost identical in the presence/absence of KPF$_6$ (20.4 s^{-1} and 19.9 s^{-1}, respectively) supports the importance of the six-oxygen coordination environment for the K$^+$ in [8H4-K], likely allowing greater catalytic performance. These findings underscore the critical role of ligand design and metal-ion coordination in optimizing the performance of hydrogenase mimics for electrocatalytic applications.

Conclusions

[FeFe]H$_2$ase mimics **7** and **8**, which feature two [(μ-adt)Fe$_2$(CO)$_6$] moieties and two 1,2,3-triazole rings linked through PEG chains of different lengths, have been prepared to study the effect of additional basic centers on the electrocatalytic properties of [(μ-adt)Fe$_2$(CO)$_6$] derivatives in acidic media.

Compounds **7** and **8** are capable of binding alkali ions (Na$^+$, K$^+$) to form 1:1 coordination complexes, in which the oxygen atoms of the PEG moiety and the *N*3 positions of the triazole rings are involved. Through ^{1}H NMR titration experiments and electrochemical studies of **7** and **8** in the presence or absence of NaPF$_6$ or KPF$_6$, we determined the relative contributions of *N*-adt amino *versus* *N*3 triazole protonated species to the HER process in TFA. The addition of Na$^+$ ions inhibits the protonation of the triazole rings in both **7** and **8**, and their electrochemical response is primarily attributed to the species protonated at the amino adt groups. However, with K$^+$, the triazolium salts are formed in TFA, and the electrocatalytic behavior of **7** and **8** reflects the contributions from species protonated at both the triazole and amino adt groups.

A computational study of the protonated complex **8** with KPF$_6$ in the presence of TFA could explain the increase in the turnover frequency (TOF) observed for this complex (37.9 s^{-1}) compared to the TOF calculated in the absence of the potassium salt (21.0 s^{-1}). The computed complex [8H4-K], protonated in both the triazole and amino [(μ-adt)Fe$_2$(CO)$_6$] groups, is still able to coordinate the K$^+$ ion through the six *O*-PEG atoms, in a very regular pseudo-18-crown-6 structure. Since the incorporation of alkali metal ions is known to enhance the electrocatalytic activity of metal complexes, the formation of complex [8H4-K] could account for the increased TOF observed for compound **8** in TFA in the presence of KPF$_6$. These findings highlight the intricate interplay between ligand design, ion-binding fragments and their effects on catalytic behavior in acidic media. Future studies are underway to explore the incorporation of other ion-binding fragments and investigate their impact on the HER process, with the aim of further optimizing the performance of hydrogenase mimics for electrocatalytic applications.

Experimental section

General

Unless otherwise stated, all the reactions were carried out under an Ar atmosphere using anhydrous solvents. Alkynes **9**[14] and **10**[15] and azide **11**[9] were prepared according to reported protocols. ^{1}H and ^{13}C{^{1}H} NMR spectra were recorded at ambient temperature in CDCl$_3$ using Bruker 500 or 300 MHz spectrometers. Chemical shifts are expressed in part per million and are referenced to residual solvent peaks. ESI-HRMS was performed using an Agilent 6500 accurate mass spectrometer with a Q-TOF analyser. Cyclic voltammograms were recorded using a Metrohm PGSTAT302N potentiostat model. In all cases, the solutions were degassed with an argon flow and sonicated prior to electrochemical analysis. For cyclic voltammograms, a 3 mm glassy-carbon working electrode, an Ag/AgCl 3 M reference electrode, and a 2 mm Pt-wire counter electrode were used. All measurements were performed at room temperature and under an argon atmosphere in CH$_3$CN solutions containing 10^{-1} M [^{n}Bu$_4$]PF$_6$ as the supporting electrolyte, with analyte concentrations of 10^{-3} M.

4488 | *Inorg. Chem. Front.*, 2025, **12**, 4480–4493

This journal is © the Partner Organisations 2025

General procedure for the CuAAC reactions

In a round-bottom flask, 1 equiv. of the dialkyne, 2 equiv. of azide **11**, and a MeCN/THF mixture in a 1 : 1 ratio were added. The resulting suspension was bubbled with Ar for 10 minutes. Subsequently, 2 equiv. of CuI and 2 equiv. of DIPEA were added. The reaction mixture was stirred at room temperature for 72 h. The solvent was evaporated under reduced pressure, and the obtained solid was purified by column chromatography (SiO$_2$, CH$_2$Cl$_2$/MeOH 95 : 5).

Synthesis of 7. Compound **7** was synthesized following the general procedure using 102 mg (0.38 mmol) of dialkyne **3**, 381 mg (0.76 mmol) of **11**, 18 mL of the solvent mixture, 145 mg (0.76 mmol) of CuI, and 0.13 mL (0.76 mmol) of DIPEA. After purification, **7** was obtained as a red solid with a yield of 92% (444 mg, 0.35 mmol). ^{1}H NMR (300 MHz, CDCl$_3$) δ: 7.96 (s, 2H, CH$_{triazole}$), 7.67 (d, J = 8.8 Hz, 4H, CH$_{Ar}$), 6.85 (d, J = 8.8 Hz, 4H, CH$_{Ar}$), 4.76 (s, 4H, OCH$_2$C$_{triazole}$), 4.35 (s, 8H, NCH$_2$S,), 3.75–3.67 (m, 16H, CH$_2$) ppm. ^{13}C{^{1}H} NMR (75 MHz, CDCl$_3$) δ: 206.9 (CO), 145.9 (C$_{triazole}$), 144.9 (C$_{Ar}$), 130.1 (C$_{Ar}$), 122.5 (CH$_{Ar}$), 120.9 (CH$_{triazole}$), 116.4 (CH$_{Ar}$), 70.7 (CH$_2$), 70.0 (CH$_2$), 64.8 (OCH$_2$C$_{triazole}$), 49.8 (SCH$_2$N) ppm. FTIR (film): $\nu_{C\equiv O}$ 2073, 2031 and 1992 cm^{-1}. HRMS-ESI m/z: calcd for C$_{42}$H$_{39}$Fe$_4$N$_8$O$_{17}$S$_4$ [M + H]$^+$: 1278.8714; found [M + H]$^+$: 1278.8724.

Synthesis of 8. Compound **8** was synthesized following the general procedure using 117 mg (0.37 mmol) of dialkyne **10**, 378 mg (0.75 mmol) of **11**, 18 mL of the solvent mixture, 142 mg (0.75 mmol) of CuI, and 0.13 mL (0.75 mmol) of DIPEA. After purification, **8** was obtained as a red solid with a yield of 74% (367 mg, 0.28 mmol). ^{1}H NMR (300 MHz, CDCl$_3$) δ: 7.96 (s, 2H, CH$_{triazole}$), 7.67 (d, J = 9.0 Hz, 4H, CH$_{Ar}$), 6.85 (d, J = 9.0 Hz, 4H, CH$_{Ar}$), 4.76 (s, 4H, OCH$_2$C$_{triazole}$), 4.35 (s, 8H, NCH$_2$S,), 3.75–3.66 (m, 20H, CH$_2$) ppm. ^{13}C{^{1}H} NMR (75 MHz, CDCl$_3$) δ: 206.9 (CO), 145.9 (C$_{triazole}$), 144.9 (C$_{Ar}$), 130.1 (C$_{Ar}$), 122.5 (CH$_{Ar}$), 120.9 (CH$_{triazole}$), 116.4 (CH$_{Ar}$), 70.7 (CH$_2$), 70.0 (CH$_2$), 64.8 (OCH$_2$C$_{triazole}$), 49.8 (SCH$_2$N) ppm. FTIR (film): $\nu_{C\equiv O}$ 2073, 2030 and 1991 cm^{-1}. HRMS-ESI m/z: calcd for C$_{44}$H$_{43}$Fe$_4$N$_8$O$_{18}$S$_4$ [M + H]$^+$: 1322.8976; found [M + H]$^+$: 1322.8986.

Computational details

Calculations were performed at the DFT level using the M06 functional[24] with an ultrafine integration grid[25] as implemented in Gaussian 16.[26] Fe, S, and K atoms were described using the scalar relativistic Stuttgart–Dresden SDD pseudopotential[27] and its associated double-ζ basis set complemented with a set of d- and f-polarization functions.[28] The 6-31G** basis set was used for the H, C, N, and O atoms.[29] All structures were fully optimized in acetonitrile solvent using the SMD continuum model.[24,30]

Author contributions

Miguel A. Sierra (MAS) designed the work. MAS and Alba Collado (AC) directed the research and interpreted the results.

Elena Sáez recorded all the NMR experiments and titrations. Alejandro Torres and Sergio Aguado executed the experimental part and interpreted the experimental results. Mar Gómez-Gallego executed the DFT calculations and was involved in the electrochemical studies. The manuscript was written through contributions of all authors. All authors have given approval to the final version of the manuscript.

Data availability

The data supporting this article have been included as part of the ESI.‡

Conflicts of interest

There are no conflicts to declare.

Acknowledgements

References

1 (*a*) J. C. Fontecilla-Camps, A. Volbeda, C. Cavazza and Y. Nicolet, Structure/function relationships of [NiFe]- and [FeFe]-hydrogenases, *Chem. Rev.*, 2007, **107**, 4273–4303; (*b*) P. M. Vignais and B. Billoud, Occurrence, classification and biological function of hydrogenases: an overview, *Chem. Rev.*, 2007, **107**, 4206–4272; (*c*) W. Lubitz, H. Ogata, O. Rüdiger and E. Reijerse, Hydrogenases, *Chem. Rev.*, 2014, **114**, 4081–4148.

2 (*a*) C. Esmieu, M. Guo, H. J. Redman, M. Lundberg and G. Berggren, Synthesis of a miniaturized [FeFe] hydrogenase model system, *Dalton Trans.*, 2019, **48**, 2280–2284; (*b*) M. Senger, S. Mebs, J. Duan, O. Shulenina, K. Laun, L. Kertess, F. Wittkamp, U.-P. Apfel, T. Happe, M. Winkler, M. Haumann and S. T. Stripp, Protonation/reduction dynamics at the [4Fe-4S] cluster of the hydrogen-forming cofactor in [FeFe]-hydrogenases, *Phys. Chem. Chem. Phys.*, 2018, **20**, 3128–3140; (*c*) P. Rodríguez-Maciá, L. Kertess, J. Burnik, J. A. Birrell, E. Hofmann, W. Lubitz, T. Happe and O. Rüdiger, His-ligation to the [4Fe-4S] subcluster tunes the catalytic bias of [FeFe] hydrogenase, *J. Am. Chem. Soc.*, 2019, **141**, 472–481; (*d*) A. J. Pierik, M. Hulstein, W. R. Hagen and S. P. Albracht, A Low-Spin Iron with CN and CO as Intrinsic Ligands Forms the Core of the Active Site in [Fe]-Hydrogenases, *Eur. J. Biochem.*, 1998, **258**, 572–578; (*e*) A. L. De Lacey, C. Stadler, C. Cavazza, E. C. Hatchikian and V. M. Fernandez, FTIR Characterization of the Active Site of the Fe-Hydrogenase

This journal is © the Partner Organisations 2025

Inorg. Chem. Front., 2025, **12**, 4480–4493 | **4489**

from *Desulfovibrio Desulfuricans*, *J. Am. Chem. Soc.*, 2000, **122**, 11232–11233; (*f*) Y. Nicolet, A. L. De Lacey, X. Vernède, V. M. Fernandez, E. C. Hatchikian and J. C. Fontecilla-Camps, Crystallographic and FTIR Spectroscopic Evidence of Changes in Fe Coordination upon Reduction of the Active Site of the Fe-Only Hydrogenase from *Desulfovibrio Desulfuricans*, *J. Am. Chem. Soc.*, 2001, **123**, 1596–1601.

3 (*a*) M. T. Lachmann, Z. Duan, P. Rodríguez-Macía and J. A. Birrell, The missing pieces in the catalytic cycle of [FeFe]hydrogenases, *Chem. Sci.*, 2024, **15**, 14062–14080; (*b*) J. A. Birrell, P. Rodríguez-Macía, E. J. Reijerse, M. A. Martini and W. Lubitz, The catalytic cycle of [FeFe] hydrogenase: A tale of two sites, *Coord. Chem. Rev.*, 2021, **449**, e214191; (*c*) M. Senger, V. Eichmann, K. Laun, J. Duan, F. Wittkamp, G. Knör, U.-P. Apfel, T. Happe, M. Winkler, J. Heberle and S. T. Stripp, How [FeFe]-Hydrogenase Facilitates Bidirectional Proton Transfer?, *J. Am. Chem. Soc.*, 2019, **141**, 17394–17403; (*d*) J. Duan, S. Mebs, K. Laun, F. Wittkamp, J. Heberle, E. Hofmann, U.-P. Apfel, M. Winkler, M. Senger, M. Haumann and S. T. Stripp, Geometry of the Catalytic Active Site in [FeFe]-Hydrogenase Is Determined by Hydrogen Bonding and Proton Transfer, *ACS Catal.*, 2019, **9**, 9140–9149; (*e*) J. Duan, M. Senger, J. Esselborn, V. Engelbrecht, F. Wittkamp, U.-P. Apfel, E. Hofmann, S. Y. Stripp, T. Happe and M. Winkler, Crystallographic and spectroscopic assignment of the proton transfer pathway in [FeFe]-hydrogenases, *Nat. Commun.*, 2018, **9**, 4726–4737; (*f*) A. J. Cornish, K. Gärtner, H. Yang, J. W. Peters and E. L. Hegg, Mechanism of proton transfer in [FeFe]-hydrogenase from *Clostridium pasteurianum*, *J. Biol. Chem.*, 2011, **286**, 38341–38347; (*g*) H. Long, P. W. King and C. H. Chang, Proton transport in *Clostridium pasteurianum* [FeFe] hydrogenase I: a computational study, *J. Phys. Chem. B*, 2014, **118**, 890–900; (*h*) G. Hong, A. J. Cornish, E. L. Hegg and R. Pachter, On understanding proton transfer to the biocatalytic [Fe-Fe]H sub-cluster in [Fe-Fe]H$_2$ases: QM/MM MD simulations, *Biochim. Biophys. Acta, Bioenerg.*, 2011, **1807**, 510–517.

4 H. Reihlen, A. Gruhl, V. Hessling and G. Über, den photochemischen und oxidativen abbau von carbonylen, *Justus Liebigs Ann. Chem.*, 1929, **472**, 268–287.

5 (*a*) Y. Li and T. B. Rauchfuss, Synthesis of diiron(ɪ) dithiolato carbonyl complexes, *Chem. Rev.*, 2016, **116**, 7043–7077; (*b*) D. Schilter, J. M. Camara, M. T. Huynh, S. Hammes-Schiffer and T. B. Rauchfuss, Hydrogenase enzymes and their synthetic models: the role of metal hydrides, *Chem. Rev.*, 2016, **116**, 8693–8749.

6 M. Y. Darensbourg, E. J. Lyon, X. Zhao and I. P. Georgakaki, The Organometallic Active Site of [Fe] Hydrogenase: Models and Entatic States, *Proc. Natl. Acad. Sci. U. S. A.*, 2003, **100**, 3683–3688.

7 See for example: (*a*) R. Mejia-Rodriguez, D. Chong, J. H. Reibenspies, M. P. Soriaga and M. Y. Darensbourg, The Hydrophilic Phosphatriazaadamantane Ligand in the Development of H$_2$ Production Electrocatalysts: Iron

Hydrogenase Model Complexes, *J. Am. Chem. Soc.*, 2004, **126**, 12004–12014; (*b*) T. Liu, M. Wang, Z. Shi, H. Cui, W. Dong, J. Chen, B. Åkermark and L. Sun, Synthesis, Structures and Electrochemical Properties of Nitro- and Amino- Functionalized Diiron Azadithiolates as Active Site Models of Fe-Only Hydrogenases, *Chem. – Eur. J.*, 2004, **10**, 4474–4479; (*c*) J. F. Capon, F. Gloaguen, P. Schollhammer and J. Talarmin, Catalysis of the Electrochemical H$_2$ evolution by Di-Iron Sub-Site Models, *Coord. Chem. Rev.*, 2005, **249**, 1664–1676; (*d*) G. A. N. Felton, A. K. Vannucci, J. Chen, L. T. Lockett, N. Okumura, B. J. Petro, U. I. Zakai, D. H. Evans, R. S. Glass and D. L. Lichtenberger, Hydrogen Generation from Weak Acids: Electrochemical and Computational Studies of a Diiron Hydrogenase Mimic, *J. Am. Chem. Soc.*, 2007, **129**, 12521–12530; (*e*) R. Zaffaroni, T. B. Rauchfuss, D. L. Gray, L. De Gioia and G. Zampella, Terminal vs Bridging Hydrides of Diiron Dithiolates: Protonation of Fe$_2$(dithiolate)(CO)$_2$(PMe$_3$)$_4$, *J. Am. Chem. Soc.*, 2012, **134**, 19260–19269; (*f*) M. T. Huynh, W. Wang, T. B. Rauchfuss and S. Hammes-Schiffer, Computational Investigation of [FeFe]-Hydrogenase Models: Characterization of Singly and Doubly Protonated Intermediates and Mechanistic Insights, *Inorg. Chem.*, 2014, **53**, 10301–10311; (*g*) A. Jablonskyte, L. R. Webster, T. R. Simmons, J. A. Wright and C. J. Pickett, Electronic Control of the Protonation Rates of Fe–Fe Bonds, *J. Am. Chem. Soc.*, 2014, **136**, 13038–13044.

8 For the synthesis of [FeFe]-H$_2$ase mimics bearing pendant basic centers, see: (*a*) J. T. Kleinhaus, F. Wittkamp, S. Yadav, D. Siegmund and U.-P. Apfel, [FeFe]-Hydrogenases: maturation and reactivity of enzymatic systems and overview of biomimetic models, *Chem. Soc. Rev.*, 2021, **50**, 1668–1784; (*b*) G. Hogarth, An unexpected leading role for [Fe$_2$(CO)$_6$(μ-pdt)] in our understanding of [FeFe]-H$_2$ases and the search for clean hydrogen production, *Coord. Chem. Rev.*, 2023, **490**, e215174 See also ref. 5*a*. Examples of the study of the effect of the additional basic centers on the electrocatalysis of these mimics: (*c*) I. O. Shotonwa, O. Ejeromedoghene, A. O. Adesoji, Y. A. Alli, C. Akinremi and S. Adewuyi, Electrochemistry, electrocatalysis, and mechanistic details into hydrogen evolution pathways of hexacoordinated iron scaffolds in hydrogenase mimics, *J. Electroanal. Chem.*, 2023, **938**, e117446; (*d*) G. R. F. Orton, S. Belazregue, J. K. Cockcroft, F. Hartl and G. Hogarth, Biomimics of [FeFe]-hydrogenases with a pendant amine: Diphosphine complexes [Fe$_2$(CO)$_4${μ-S(CH$_2$)$_n$S}{κ2-(Ph$_2$PCH$_2$)$_2$NR}] (n = 2, 3; R = Me, Bn) towards H2 oxidation catalysts, *J. Organomet. Chem.*, 2023, **991**, 122673; (*e*) A. Mele, F. Arrigoni, C. Elleouet, F. Y. Pétillon, P. Schollhammer and G. Zampella, Insights into Triazolylidene Ligands Behaviour at a Di-Iron Site Related to [FeFe]-Hydrogenases, *Molecules*, 2022, **27**, 4700; (*f*) A. Mele, S. Bertini, M. Albrecht, C. Elleouet, F. Y. Pétillon and P. A. Schollhammer, Diiron Hydrogenase Mimic Featuring a 1,2,3-Triazolylidene, *Chimia*, 2020, **74**, 499–503; (*g*) R. Zaffaroni, W. I. Dzik, R. J. Detz, J. I. van der

4490 | *Inorg. Chem. Front.*, 2025, **12**, 4480–4493

This journal is © the Partner Organisations 2025

Vlugt and J. N. H. Reek, Proton Relay Effects in Pyridyl-Appended Hydrogenase Mimics, *Eur. J. Inorg. Chem.*, 2019, 2498–2509; (*h*) R. Becker, S. Amirjalayer, P. Li, S. Woutersen and J. N. Reek, An iron-iron hydrogenase mimic with appended electron reservoir for efficient proton reduction in aqueous media, *Sci. Adv.*, 2016, **2**, e1501014; (*i*) N. Wang, M. Wang, J. H. Liu, K. Jin, L. Chen and L. C. Sun, Preparation, Facile Deprotonation and Rapid H/D Exchange of the μ-Hydride Diiron Model Complexes of the [FeFe]-Hydrogenase Containing a Pendant Amine in a Chelating Diphosphine Ligand, *Inorg. Chem.*, 2009, **48**, 11551–11558; (*j*) N. Wen, F.-F. Xu, R.-P. Chen and S.-W. Du, Reversible carbonylation of [2Fe2S] model complexes with pendant quinoline or pyridine arms, *J. Organomet. Chem.*, 2014, **756**, 61–67; (*k*) J. A. Birrell, P. Rodríguez-Maciá, E. J. Reijerse, M. A. Martini and W. Lubitz, The catalytic cycle of [FeFe] hydrogenase: A tale of two sites, *Coord. Chem. Rev.*, 2021, **449**, 214191; (*l*) L. Greene, G. E. Vansuch, B. C. Chica, M. W. W. Adams and R. Brian Dyer, Applications of Photogating and Time Resolved Spectroscopy to Mechanistic Studies of Hydrogenases, *Acc. Chem. Res.*, 2017, **50**, 2718–2726; (*m*) O. Lampret, A. Adamska-Venkatesh, H. Konegger, F. Wittkamp, U.-P. Apfel, E. J. Reijerse, W. Lubitz, O. Rüdiger, T. Happe and M. Winkler, Interplay between CN- Ligands and the Secondary Coordination Sphere of the H-Cluster in [FeFe]-Hydrogenases, *J. Am. Chem. Soc.*, 2017, **139**, 18222–18230.

9 A. D. Merinero, A. Collado, L. Casarrubios, M. Gómez-Gallego, C. Ramírez de Arellano, A. Caballero, F. Zapata and M. A. Sierra, Triazole-Containing [FeFe]-Hydrogenase Mimics: Synthesis and Electrocatalytic Behavior, *Inorg. Chem.*, 2019, **58**, 16267–16278.

10 See, among others: (*a*) M. S. Somachandra, B. Averkiev and P. E. Sues, Unsymmetric Co-Facial "Salixpyrrole" Hydrogen Evolution Catalysts: Two Metals are Better than One, *Inorg. Chem.*, 2024, **63**, 13346–11335; (*b*) R. R. Golwankar, A. Kumar, V. W. Day and J. D. Blakemore, Revealing the Influence of Diverse Secondary Metal Cations on Redox-Active Palladium Complexes, *Chem. – Eur. J.*, 2022, **28**, e202200344; (*c*) H. Shao, S. K. Muduli, P. D. Tran and H. S. Soo, Enhancing electrocatalytic hydrogen evolution by nickel salicylaldimine complexes with alkali metal cations in aqueous media, *Chem. Commun.*, 2016, **52**, 294–2951; (*d*) D. C. Lacy, Y. J. Park, J. W. Ziller, J. Yano and A. S. Borovik, Assembly and Properties of Heterobimetallic CoII/III/CaII Complexes with Aquo and Hydroxo Ligands, *J. Am. Chem. Soc.*, 2012, **134**, 17526–17535; (*e*) Y. J. Park, J. W. Ziller and A. S. Borovik, The Effects of Redox-Inactive Metal Ions on the Activation of Dioxygen: Isolation and Characterization of a Heterobimetallic Complex Containing a MnIII–(μ-OH)–CaII Core, *J. Am. Chem. Soc.*, 2011, **133**, 9258–9261; (*f*) S. Haaf, E. Kaifer, H. Wadepohl and H.-J. Himmel, Use of Crown Ether Functions as Secondary Coordination Spheres for the Manipulation of Ligand–Metal Intramolecular Electron Transfer in Copper–Guanidine Complexes, *Chem. – Eur. J.*, 2021, **27**, 959–970;

(*g*) S. Bang, Y.-M. Lee, S. Hong, K.-B. Cho, Y. Nishida, M. S. Seo, R. Sarangi, S. Fukuzumi and W. Nam, Redox-inactive metal ions modulate the reactivity and oxygen release of mononuclear non-heme iron(III)–peroxo complexes, *Nat. Chem.*, 2014, **6**, 934–940.

11 (*a*) A. Torres, A. Collado, M. Gómez-Gallego, C. Ramírez de Arellano and M. A. Sierra, Heteropolymetallic [FeFe]-Hydrogenase Mimics: Synthesis and Electrochemical Properties, *Inorg. Chem.*, 2023, **62**, 3409–3419; (*b*) S. Aguado, M. Gómez-Gallego, L. Casarrubios and M. A. Sierra, Electrocatalytic HER Performance of [FeFe]-Hydrogenase Mimics Bearing M-salen Moieties (M=Zn, Ni, Fe, Mn), *Chem. – Eur. J.*, 2025, e202403721.

12 (*a*) J. M. Lehn, *Supramolecular Chemistry: Concepts and Perspectives*, Wiley-VCH, Weinheim, 1995; (*b*) R. M. Izatt, K. Pawlak, J. S. Bradsshaw and R. L. Bruening, Thermodynamic and Kinetic Data for Macrocycle Interaction with Cations, Anions, and Neutral Molecules, *Chem. Rev.*, 1995, **95**, 2529–2586; (*c*) R. Peng, Y. Xu and Q. Cao, Recent advances in click-derived macrocycles for ions recognition, *Chin. Chem. Lett.*, 2018, **29**, 1465–1474; (*d*) J. W. Steed, First- and second-sphere coordination chemistry of alkali metal crown ether complexes, *Coord. Chem. Rev.*, 2001, **215**, 171–221; (*e*) N. A. Itsikson, G. L. Rusinov, D. G. Beresnev and O. L. Chupakhin, Modification of macrocyclic compounds by Azaheterocycles, *Heterocycles*, 2003, **61**, 593–637.

13 (*a*) V. V. Rostovtsev, L. G. Green, V. V. Fokin and K. B. A. Sharpless, Stepwise Huisgen Cycloaddition Process: Copper(I)-Catalyzed Regioselective "Ligation" of Azides and Terminal Alkynes, *Angew. Chem., Int. Ed.*, 2002, **41**, 2596–2599; (*b*) C. W. Torne, C. Christensen and M. Meldal, Peptidotriazoles on Solid Phase: [1,2,3]-Triazoles by Regiospecific Copper(I)-Catalyzed 1,3-Dipolar Cycloadditions of Terminal Alkynes to Azides, *J. Org. Chem.*, 2002, **67**, 3057–3064; (*c*) H. C. Kolb, M. G. Finn and K. B. Sharpless, Click Chemistry: Diverse Chemical Function from a Few Good Reactions, *Angew. Chem., Int. Ed.*, 2001, **40**, 2004–2021; (*d*) M. Meldal and C. W. Torne, Cu-Catalyzed Azide-Alkyne Cycloaddition, *Chem. Rev.*, 2008, **108**, 2952–3015.

14 T. Koopmans, T. M. Wood, P. 't Hart, L. H. J. Kleijn, A. P. A. Hendrickx, R. J. L. Willems, E. Breukink and N. I. Martin, Semisynthetic lipopeptides derived from nisin display antibacterial activity and lipid II binding on par with that of the parent compound, *J. Am. Chem. Soc.*, 2015, **137**, 9382–9389.

15 P. J. Jervis, M. Moulis, J.-P. Jukes, H. Ghadbane, L. R. Cox, V. Cerundolo and G. S. Besra, Towards multivalent CD1d ligands: synthesis and biological activity of homodimeric α-galactosyl ceramide analogues, *Carbohydr. Res.*, 2012, **356**, 152–162.

16 C. J. Pedersen, Cyclic polyethers and their complexes with metal salts, *J. Am. Chem. Soc.*, 1967, **89**, 7017–7036.

17 T. Terashima, M. Kawabe, Y. Miyabara, H. Yoda and M. Sawamoto, Polymeric pseudo-crown ether for cation recognition via cation template-assisted cyclopolymerization, *Nat. Commun.*, 2013, **4**, 2321.

This journal is © the Partner Organisations 2025

Inorg. Chem. Front., 2025, **12**, 4480–4493 | **4491**

18 The reported values ($\log K_a$) of the association constants of crown ethers with Na^+ and K^+ are deeply influenced by the solvent. See: (*a*) H. K. Frensdorff, Stability constants of cyclic polyether complexes with univalent cations, *J. Am. Chem. Soc.*, 1971, **93**, 600–606; (*b*) D. M. Dishong and G. W. Gokel, Crown Cation Complex Effects. 16. Solvent Dependence of the 15-Crown-5 and 18-Crown-6 Equilibria with Sodium Cation, *J. Org. Chem.*, 1982, **47**, 147–148; (*c*) J. D. Lin and A. I. Popov, Nuclear Magnetic Resonance Studies of Some Sodium Ion Complexes with Crown Ethers and Cryptands in Various Solvents, *J. Am. Chem. Soc.*, 1981, **103**, 3173–3111; (*d*) I. M. Kolthoff and M. K. Chantooni Jr., Transfer Activity Coefficients in Various Solvents of Severaln Univalent Cations Complexed with Dibenzo-18-crown-6, *Anal. Chem.*, 1980, **52**, 1039–1044; (*e*) I. Inoue, Y. Liu, L.-H. Tong, M. Ouchi and T. Hakushi, Complexation Thermodynamics of Crown Ethers. Part 3. 12-Crown-4 to 36-Crown-12: from Rigid to Flexible Ligand, *J. Chem. Soc., Perkin Trans. 2*, 1993, 1947–1950.

19 L. Fabbrizi, The experimental average Na-O distance in crown ethers is 2.47–2.54 Å. The average K-O distance is 2.80 Å, in *Cryptands and Cryptates*, World Scientific Publishing Europe Ltd., 2018.

20 (*a*) Z. Xiao, Z. Wei, L. Long, Y. Wang, D. J. Evans and X. Liu, Diiron Carbonyl Complexes Possessing a Fe(ɪɪ)Fe(ɪɪ) Core: Synthesis, Characterization and electrochemical Investigation, *Dalton Trans.*, 2011, **40**, 4291–4299; (*b*) S. Dey, A. Rana, S. G. Dey and A. Dey, Electrochemical Hydrogen Production in Acidic Water by an Azadithiolate Bridged Synthetic Hydrogenase Mimic: Role of Aqueous Solvation in Lowering Overpotential, *ACS Catal.*, 2013, **3**, 429–436; (*c*) A. Rana, P. K. Das, B. Mondal, S. Dey, D. Crouthers and A. Dey, Investigation of Bridgehead Effects on Reduction Potential in Alkyl and Aryl Azadithiolate-Bridged (μ-SCH_2XCH_2S) [$Fe(CO)_3$]$_2$ Synthetic Analogues of [FeFe]-H_2ase Active Site, *Eur. J. Inorg. Chem.*, 2018, 3633–3643; (*d*) D. Chong, I. P. Georgakaki, R. Mejia-Rodriguez, J. Sanabria-Chinchilla, M. P. Soriaga and M. Y. Darensbourg, Electrocatalysis of Hydrogen Production by Active Site Analogues of the Iron Hydrogenase Enzyme: Structure/Function Relationships, *J. Chem. Soc., Dalton Trans.*, 2003, 4158–4163.

21 (*a*) J.-F. Capon, S. Ezzaher, F. Gloaguen, F. Y. Pétillon, P. Schollhammer and J. Talarmin, Electrochemical insights into the mechanisms of proton reduction by [$Fe_2(CO)_6$\{μ-$SCH_2N(R)CH_2S$\}] complexes related to the [2Fe]H subsite of [FeFe]hydrogenase, *Chem. – Eur. J.*, 2008, **14**, 1954–1964; (*b*) F. Gloaguen, J. D. Lawrence, T. B. Rauchfuss, M. Bénard and M. Rohmer, Bimetallic Carbonyl Thiolates as Functional Models for Fe-Only Hydrogenases, *Inorg. Chem.*, 2002, **41**, 6573–6582; (*c*) J.-F. Capon, F. Gloaguen, P. Schollhammer and J. Talarmin, Electrochemical Proton Reduction by Thiolate-Bridged Hexacarbonyldiiron Clusters, *J. Electroanal. Chem.*, 2004, **566**, 241–247; (*d*) J.-F. Capon, F. Gloaguen, P. Schollhammer and J. Talarmin, Activation of Proton by the Two-Electron Reduction of a Diiron Organometallic Complex, *J. Electroanal. Chem.*, 2006, **595**, 47–52; (*e*) S. J. Borg, T. Behrsing, S. P. Best, M. Razavet, X. Liu and C. J. Pickett, Electron Transfer at a Dithiolate-Bridged Diiron Assembly: Electrocatalytic Hydrogen Evolution, *J. Am. Chem. Soc.*, 2004, **126**, 16988–16999.

22 (*a*) N. D. Lowe and C. D. Garner, Transition-metal Complexes of Crown Ether Benzodithiolenes, *J. Chem. Soc. Dalton Trans.*, 1993, 2197–2207; (*b*) N. D. Lowe and C. D. Garner, Transition-metal Complexes of Crown Ether Benzodithiolenes. Part 2. The Effects of Alkali-metal Cation Binding, *J. Chem. Soc., Dalton Trans.*, 1993, 3333–3340; (*c*) H. M. Nguyen, H. W. T. Morgan, T. Chantarojsiri, T. A. Kerr, J. Y. Yang, A. N. Alexandrova and N. G. Léonard, Charge and Solvent Effects on the Redox Behavior of Vanadyl Salen-Crown Complexes, *J. Phys. Chem. A*, 2023, **127**, 5324–5334; (*d*) J. L. Alvarez-Hernandez, X. Zhang, K. Cui, A. P. Deziel, S. Hammes-Schiffer, N. Hazari, N. Piekut and M. Zhong, Long-range electrostatic effects from intramolecular Lewis acid binding influence the redox properties of cobalt–porphyrin complexes, *Chem. Sci.*, 2024, **15**, 6800–6815.

23 R. D. Shannon, Revised Effective Ionic Radii and Systematic Studies of Interatomic Distances in Halides and Chaleogenides, *Acta Crystallogr., Sect. A*, 1976, **32**, 751–767.

24 Y. Zhao and D. G. Truhlar, The M06 suite of density functionals for main group thermochemistry, thermochemical kinetics, noncovalent interactions, excited states, and transition elements: two new functionals and systematic testing of four M06-class functionals and 12 other functionals, *Theor. Chem. Acc.*, 2008, **120**, 215–241.

25 (*a*) Y. Zhao and D. G. Truhlar, Density functionals with broad applicability in Chemistry, *Acc. Chem. Res.*, 2008, **41**, 157–167; (*b*) Y. Zhao and D. G. Truhlar, Applications and validations of the Minnesota density functionals, *Chem. Phys. Lett.*, 2011, **502**, 1–13.

26 M. J. Frisch, G. W. Trucks, H. B. Schlegel, G. E. Scuseria, M. A. Robb, J. R. Cheeseman, G. Scalmani, V. Barone, G. A. Petersson, H. Nakatsuji, X. Li, M. Caricato, A. V. Marenich, J. Bloino, B. G. Janesko, R. Gomperts, B. Mennucci, H. P. Hratchian, J. V. Ortiz, A. F. Izmaylov, J. L. Sonnenberg, D. Williams-Young, F. Ding, F. Lipparini, F. Egidi, J. Goings, B. Peng, A. Petrone, T. Henderson, D. Ranasinghe, V. G. Zakrzewski, J. Gao, N. Rega, G. Zheng, W. Liang, M. Hada, M. Ehara, K. Toyota, R. Fukuda, J. Hasegawa, M. Ishida, T. Nakajima, Y. Honda, O. Kitao, H. Nakai, T. Vreven, K. Throssell, J. A. Montgomery Jr., J. E. Peralta, F. Ogliaro, M. J. Bearpark, J. J. Heyd, E. N. Brothers, K. N. Kudin, V. N. Staroverov, T. A. Keith, R. Kobayashi, J. Normand, K. Raghavachari, A. P. Rendell, J. C. Burant, S. S. Iyengar, J. Tomasi, M. Cossi, J. M. Millam, M. Klene, C. Adamo, R. Cammi, J. W. Ochterski, R. L. Martin, K. Morokuma, O. Farkas, J. B. Foresman and D. J. Fox, *Gaussian 16, Revision C.01*, Gaussian, Inc., Wallingford CT, 2016.

4492 | *Inorg. Chem. Front.*, 2025, **12**, 4480–4493

This journal is © the Partner Organisations 2025

27 U. Andrae, M. Häußermann, H. Dolg, H. Stoll and H. Preuß, Energy-adjusted ab initio pseudopotentials for the second and third row transition elements, *Theor. Chim. Acta*, 1990, **77**, 123–141.

28 (*a*) A. W. Ehlers, M. Böhme, S. Dapprich, A. Gobbi, A. Höllwarth, V. Jonas, K. F. Köhler, R. Stegmann, A. Veldkamp and G. Frenking, A set of f-polarization functions for pseudo-potential basis sets of the transition metals Sc-Cu, Y-Ag and La-Au, *Chem. Phys. Lett.*, 1993, **208**, 111; (*b*) A. Höllwarth, M. Biihme, S. Dapprich, A. W. Ehlers, A. Gobbi, V. Jonas, K. F. Kijhler, R. Stegmann, A. Veldkamp and G. Frenking, A set of d-polarization functions for pseudo-potential basis sets of the main group elements Al-Bi and f-type polarization functions for Zn, Cd, Hg, *Chem. Phys. Lett.*, 1993, **208**, 237–240.

29 (*a*) W. J. Hehre, R. J. Ditchfield and A. Pople, Self-Consistent molecular orbital methods. XII. Further extensions of Gaussian-Type basis sets for use in molecular orbital studies of organic molecules, *J. Chem. Phys.*, 1972, **56**, 2257–2261; (*b*) M. M. Francl, W. J. Pietro, W. J. Hehre, J. S. Binkley, M. S. Gordon, D. J. J. DeFrees and A. Pople, Self-consistent molecular orbital methods. XXIII. A polarization-type basis set for second-row elements, *J. Chem. Phys.*, 1982, **77**, 3654–3665.

30 A. V. Marenich, C. J. Cramer and D. G. Truhlar, Universal solvation model based on solute electron density and on a continuum model of the solvent defined by the bulk dielectric constant and atomic surface tensions, *J. Phys. Chem. B*, 2009, **113**, 6378–6396.

This journal is © the Partner Organisations 2025

Inorg. Chem. Front., 2025, **12**, 4480–4493 | **4493**